Available online at www.sciencedirect.com
SCIENCE DIRECT®
PERGAMON
International Journal of Heat and Mass Transfer 46 (2003) 4669–4679
International Journal of HEAT and MASS TRANSFER
www.elsevier.com/locate/ijhmt

Analysis of film condensation heat transfer inside a vertical micro tube with consideration of the meniscus draining effect

X.Z. Du, T.S. Zhao *

Department of Mechanical Engineering, The Hong Kong University of Science and Technology, Clear Water Bay, Kowloon, Hong Kong, China

Received 21 January 2003; received in revised form 16 May 2003

Abstract

In this paper we report on a theoretical analysis of film condensation heat transfer in a vertical micro tube with a thin metal wire welded on its inner surface. Both the radial and the axial distributions of condensate liquid along the tube wall and over the meniscus zone, formed by the wire in contact with the tube inner surface, are determined based on the minimum energy principle over the liquid–vapor two-phase flow system. The influences of the contact angle between the condensate liquid and the channel wall as well as the wire diameter on the condensate distributions and the heat transfer characteristics are examined. It is found that an increase in the wire diameter results in significant enhancement of heat transfer in the channel. It is also demonstrated that the wettability between the wire and the condensate has a little influence on the overall heat transfer coefficients, although it affects the condensate liquid distribution. Compared to a round tube with the same inside diameter, significant enhancement of condensation heat transfer is found for the present configured microchannel.

1. Introduction

The study of condensation heat transfer in microchannels is important for the design and optimization of heat pipes and capillary pumped loops (CPL), which have been demonstrated to be the most promising devices as the efficient and integrated packaging–cooling schemes for ultra-fast electronic devices and other microsystems. It has recently been demonstrated that the heat transfer rates can be rather high when condensation takes place in micro/mini channels with non-circular cross sections [1–4]. One of the major reasons for the high heat transfer rates for condensation in non-circular channels is that thinning the liquid film thickness due to the meniscus effect, induced by the sharp corners of the non-circular channel, leads to the reduction in the thermal resistance [2]. The subject of this paper is also concerned with condensation heat transfer in non-circular channels.

The majority of early studies of condensation heat transfer inside non-circular microchannels have been confined to the studies of micro heat pipes. Khrustalev and Faghri [3] developed a detailed mathematical model to examine the heat and mass transfer processes in a micro heat pipe. The liquid flow in the triangular-shaped corners with a polygonal cross section was considered by accounting for the variation of the curvature of the free liquid surface and the interfacial shear stresses due to a liquid–vapor frictional interaction. Sartre et al. [5] presented a three-dimensional steady-state model for predicting heat transfer in a micro heat pipe array. By solving the meniscus region equations, the two-dimensional wall heat conduction problem and the longitudinal capillary two-phase flow, they showed that the draining effect through the meniscus region played an

* Corresponding author. Tel.: +852-2358-8647; fax: +852-2358-1543.
E-mail address: metzhao@ust.hk (T.S. Zhao).

0017-9310/$ - see front matter © 2003 Elsevier Ltd. All rights reserved.
doi:10.1016/S0017-9310(03)00293-X

Nomenclature

A	cross-section area, m^2
c_f	friction coefficient
D	diameter, m
E	energy per unit length, W/m
g	gravity acceleration, m^2/s
h	heat transfer coefficient, $W/m^2\,K$
h_{lv}	latent heat, J/kg
$\dot{m}$	mass flow rate, kg/s
Nu	Nusselt number
P	periphery length, m
p	pressure, pa
u	axial velocity, m/s
v	circumferential velocity, m/s
R	radius, m
Re	Reynolds number
r	radial coordinate
r_m	radius of meniscus, m
T	temperature, K
x	vapor quality
z	axial coordinate

Greek symbols

α	contact angle
δ	thickness, m
Θ	azimuthal angle
θ	polar angle
λ	conductivity, W/m K
μ	dynamic viscosity, $N/s\,m^2$
ρ	density, kg/m^3
σ	surface tension, N/m
τ	shear stress, N/m^2

Subscripts

0	initial
h	hydraulic
i	inside of tube
k	kinetic energy
l	condensate liquid
lv	vapor–liquid interface
m	meniscus zone or mass
o	outside of metal wire
u	fluid flow
s	surface energy
T	total
v	vapor
w	tube wall
δ	liquid film surface

important role for phase change. For vapor and liquid flow in a micro heat pipe with triangular channels, Sobhan et al. [6] derived the governing equations taking into account the variation in the flow cross-sectional areas of the vapor and liquid phases and incorporating the phase change during the process. Peterson and his co-workers conducted a number of studies on heat transfer characteristics of micro heat pipes. Swanson and Peterson [7] proposed a thermodynamic model of the vapor–liquid interface in micro heat pipes, including the changes in local interfacial curvature and Marangoni effects. Relationships were developed for the interfacial mass flux in an extended meniscus, as well as the heat transfer rate in the intrinsic meniscus. Ha and Peterson [8] proposed a re-evaluated semi-empirical analytical model for predicting the maximum heat transport capacity in micro heat pipes considering the meniscus corner effect. And Peterson and Ma [9,10] also developed the mathematical models for predicting the heat transport capability and temperature gradients that contributed to the overall axial temperature drop as a function of heat transfer in a micro heat pipe.

The existence of the meniscus corner zone also plays an important role on the condensate film distribution, which has an obvious impact on the condensation heat transfer characteristics. Zhang and Faghri [4] investigated condensation in a capillary grooved channel. Condensation on the fin top and at the meniscus region was modeled by introducing additional source terms in the continuity, and energy equations. Yang [11] provided a critical review of existing prediction models to correlate condensation heat transfer coefficients, including gravity-force dominated models, vapor-shear dominated models and the effects of the surface-tension force. And they themselves also developed an analytical model to account for the effects of vapor and surface tension forces, simultaneously [12]. Webb and Zhang [13] discussed the ability of the existing accepted correlations to predict single-phase and two-phase heat transfer and friction in channels having small hydraulic diameters, where capillary force should be taken into consideration. Wang et al. [14] documented local convection heat transfer and flow regime measurements for HFG-134a condensing inside a horizontal rectangular multi-port aluminum condenser tube of 1.46 mm hydraulic diameter. Their experiments suggested that liquid drawn into the meniscus corners of the tube altered the phase distribution in the annular flow regime and stabilized the annular flow regime at lower vapor velocities. Tabatabai and Faghri [15] developed a flow map to predict the effects of surface tension on two-phase flow patterns in horizontal miniature and micro tubes to show how each regime transition boundary is affected by the capillary force.

Micro/mini channels with triangular, rectangular, and H-shaped cross sections can be formed by aluminum extrusion and brazing processes, which are usually complicated and expensive. In this work, we introduce a new non-circular microchannel, formed by a circular micro tube with a thin metal wire welded on its inner surface. The formation of this type of non-circular microchannels is rather simple and inexpensive. The purpose of this work is to investigate analytically the film condensation heat transfer characteristics in such microchannels. The meniscus draining effect, which is a result of the wire being in contact with the tube inner surface, is examined based on the minimum energy principle over the liquid–vapor two-phase flow. The influences of the contact angle between the condensate liquid and channel wall as well as the wire diameter on the condensate distributions and the heat transfer characteristics are also discussed. We will demonstrate that the heat transfer rates can be rather high when the film condensation takes place in such a simple non-circular channel.

2. Mathematical model

Consider the film condensation for the vapor flowing downward in a vertical flow passage formed by welding a thin metal wire with radius, R_o, on the inner wall of a round micro tube with inside radius, R_i. Half of the symmetric cross section of the flow passage is illustrated in Fig. 1. The saturated vapor with a velocity, u_{v0}, and temperature, T_s, condenses along the tube inner wall and over the meniscus zone, formed by the wire in contact with the tube inner wall, as the outer tube wall is cooled isothermally at a temperature, T_w ($T_w < T_s$). We assume that the welded wire is in thermal equilibrium with the vapor and thus, no condensation takes place on the surface of the wire. As indicated in Fig. 1, the two-phase flow field over the cross-section of the flow passage can be divided into three zones: the thin liquid film zone along the tube inner wall, the meniscus zone formed by the wire in contact with the tube wall, and, the vapor core zone occupying the remainder of the cross section. As shown in Fig. 1, the two-phase flow over the tube cross section is characterized by three polar coordinates with their origins designated by O_1, O_2, and O_3, respectively. The liquid–vapor interface within the thin liquid film zone is characterized by a radius of $R_i - \delta_{l,i}$ (with $\delta_{l,i}$ denoting the local liquid film thickness) with its origin at O_1 and an angle of $\Theta_{i,m}$ starting from point A and ending at point B where the thin liquid film zone and the meniscus zone merges. Within the meniscus zone the liquid–vapor interface is characterized by a radius of r_m with its origin at O_3 and an angle of Θ_m starting from point B and ending at point M where the liquid wets the surface of the wire with a contact angle, α. Note that it is assumed that the thin liquid film at point B is tangential to the arc of the liquid–vapor interface within the meniscus zone. It is apparent that once the parameters of r_m and $\delta_{l,i}$ are determined, the liquid–vapor interface over a given cross section will be fixed. The determination of r_m and $\delta_{l,i}$ will be elaborated in a separate section. Some other geometric parameters in terms of r_m and $\delta_{l,i}$ are described below.

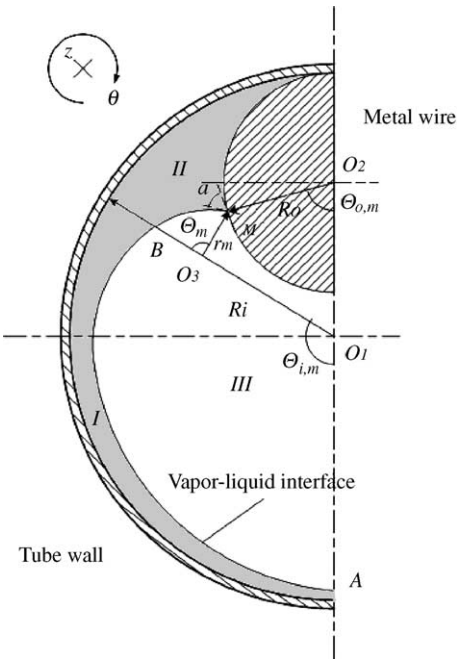

Fig. 1. Schematic of the physical problem. (I) Thin liquid film inside tube wall; (II) meniscus zone; (III) vapor flow zone.

The angle, $\Theta_{i,m}$, characterizing the width of the thin film zone, is given by

$$\Theta_{i,m} = \pi - \cos^{-1}\left(\frac{\overline{O_1O_3}^2 + \overline{O_1O_2}^2 - \overline{O_2O_3}^2}{2\overline{O_1O_3}\cdot\overline{O_1O_2}}\right), \tag{1}$$

where

$$\overline{O_1O_2} = R_i - R_o, \quad \overline{O_1O_3} = R_i - r_m - \delta_{l,i} \tag{2}$$

and

$$\overline{O_2O_3} = [r_m^2 + R_o^2 - 2r_mR_o\cos(\pi - \alpha)]^{0.5}. \tag{3}$$

The angle, $\Theta_{o,m}$, characterizing the location of point M at the surface of the wire, can be expressed as

$$\Theta_{o,m} = \cos^{-1}\left(\frac{\overline{O_2O_3}^2 + \overline{O_1O_2}^2 - \overline{O_1O_3}^2}{2\overline{O_2O_3}\cdot\overline{O_1O_2}}\right) + \cos^{-1}\left(\frac{\overline{O_2O_3}^2 + R_i^2 - r_m^2}{2\overline{O_2O_3}\cdot R_o}\right), \tag{4}$$

while the angle, Θ_m, characterizing the width of the meniscus zone, is given by

$$\Theta_m = \pi - \cos^{-1}\left(\frac{\overline{O_2O_3}^2 + \overline{O_1O_3}^2 - \overline{O_1O_2}^2}{2\overline{O_2O_3}\cdot\overline{O_1O_3}}\right) - \cos^{-1}\left(\frac{\overline{O_2O_3}^2 + r_m^2 - R_i^2}{2\overline{O_2O_3}\cdot r_m}\right). \quad (5)$$

Finally, the cross-section area occupied by the meniscus zone can be determined from

$$A_{lm} = \frac{R_i^2}{2}(\pi - \Theta_{i,m}) - A_{O_1O_2O_3} - A_{O_2O_3M} - \frac{r_m^2}{2}\Theta_m - \frac{R_o^2}{2}(\pi - \Theta_{o,m}), \quad (6)$$

where $A_{O_1O_2O_3}$ and $A_{O_2O_3M}$ denote the triangular areas of $\Delta O_1O_2O_3$ and ΔO_2O_3M, respectively, and can be determined from the sidewall lengths given by Eqs. (2) and (3). We now analyze the condensation behavior in the thin liquid film zone and in the meniscus zone as follows.

2.1. Condensation in the thin liquid film zone

Consider the condensation behavior within the thin liquid film zone, designated by the polar coordinate (r_i, θ_i) with $R_i - \delta_{l,i} \leqslant r_i \leqslant R_i$ and $0 \leqslant \theta_i \leqslant \theta_{i,m}$. On one hand, within this zone, the condensate liquid film moves downward in the z-direction due to the gravity and the liquid–vapor interfacial shear stress. On the other hand, part of the condensate produced is also drained into the meniscus zone due to the capillary pressure difference caused by the change in the liquid–vapor interface curvature. We assume that the liquid motion is an incompressible, two-dimensional laminar flow with the constant fluid properties. For small Reynolds number flows in a microchannel considered in this work, we can write the conservation equations of mass and momentum in the thin film zone as follows:

$$\frac{1}{r_i}\frac{\partial v_{l,i}}{\partial \theta_i} + \frac{\partial u_{l,i}}{\partial z} = 0, \quad (7)$$

$$\mu_l \frac{\partial^2 v_{l,i}}{\partial r_i^2} - \frac{1}{r_i}\frac{\partial p_{l,i}}{\partial \theta_i} = 0, \quad (8)$$

where $v_{l,i}$ denotes the condensate film velocity in the azimuth coordinate, θ_i, $u_{l,i}$ is the velocity in the axial direction, z, and $p_{l,i}$ is the liquid pressure in the thin liquid film zone. The corresponding boundary conditions are given by

$$v_{l,i} = 0, \quad \text{at } r_i = R_i, \quad (9a)$$

$$\frac{\partial v_{l,i}}{\partial r_i} = 0, \quad \text{at } r_i = R_i - \delta_{l,i}. \quad (9b)$$

In the axial direction, z, the motion of the condensate liquid is governed by

$$\frac{1}{r_i}\frac{\partial}{\partial r_i}\left(r_i\mu_l\frac{\partial u_{l,i}}{\partial r_i}\right) + \rho_l g - \frac{\partial p_{l,i}}{\partial z} = 0, \quad (10)$$

with the boundary conditions given by:

$$u_{l,i} = 0, \quad \text{at } r_i = R_i, \quad (11a)$$

$$-\mu_l\frac{\partial u_{l,i}}{\partial r_i} = \tau_{\delta,i}, \quad \text{at } r_i = R_i - \delta_{l,i}, \quad (11b)$$

where $\tau_{\delta,i}$ designates the interfacial shear stress at the vapor–liquid interface.

The pressure gradient of condensate, $\frac{\partial p_{l,i}}{\partial \theta_i}$, in Eq. (8) is related to the vapor pressure gradient by the Young–Laplace equation, i.e.:

$$\frac{\partial p_{l,i}}{\partial \theta_i} = \frac{\partial}{\partial \theta_i}\left(p_v - \frac{\sigma_{lv}}{R_i - \delta_{l,i}}\right), \quad (12)$$

where σ_{lv} is surface tension at the liquid–vapor interface. Assuming that the vapor pressure, p_v, is constant over the vapor core zone (zone III), we can rewrite Eq. (12) as

$$\frac{\partial p_{l,i}}{\partial \theta_i} = -\frac{\sigma_{lv}}{(R_i - \delta_{l,i})^2}\frac{\partial \delta_{l,i}}{\partial \theta_i}. \quad (13)$$

Inserting Eq. (13) into Eq. (8) and performing integration subject to the boundary conditions Eqs. (9) give

$$v_{l,i} = \frac{1}{\mu_l}\frac{\partial p_{l,i}}{\partial \theta_i}\left(r_i \ln\frac{r_i}{R_i - \delta_{l,i}} - R_i \ln\frac{R_i}{R_i - \delta_{l,i}} - r_i + R_i\right). \quad (14)$$

Similarly, in the axial direction, the pressure gradient of condensate, $\frac{\partial p_{l,i}}{\partial z}$, is also related to the vapor pressure gradient, $\frac{\partial p_v}{\partial z}$, by the Young–Laplace equation, i.e.:

$$\frac{\partial p_{l,i}}{\partial z} = \frac{\partial}{\partial z}\left(p_v - \frac{\sigma_{lv}}{R_i - \delta_{l,i}}\right). \quad (15)$$

For the case when the inertial effect is negligibly small, the pressure gradient of the vapor flow along the axial direction is balanced by the gravitational force and the shear stress between the vapor and liquid, i.e.:

$$\frac{dp_v}{dz} = \rho_v g - \frac{\tau_{\delta,i}P_w}{A_v}, \quad (16)$$

where P_w is the perimeter of the vapor core zone at an axial position z, and A_v is the cross-section area of the vapor core zone. Combining Eqs. (15) and (16) yields

$$\frac{\partial p_{l,i}}{\partial z} = \rho_v g - \frac{\tau_{\delta,i}P_w}{A_v} + \frac{\sigma_{lv}}{(R_i - \delta_{l,i})^2}\frac{d(R_i - \delta_{l,i})}{dz}. \quad (17)$$

Note that the shear stress at the liquid–vapor interface, $\tau_{\delta,i}$, is in part due to the momentum transfer caused by the condensation,

$$\tau_{\delta,\mathrm{im}} = \frac{1}{(R_\mathrm{i}-\delta_{\mathrm{l,i}})}\frac{\partial^2 \dot{m}_{\mathrm{l,i}}}{\partial z \partial \theta_\mathrm{i}}(u_\mathrm{v}-u_{\mathrm{l},i\delta}) \tag{18a}$$

and in part due to the velocity difference at the liquid–vapor interface,

$$\tau_{\delta,\mathrm{iu}} = \frac{c_\mathrm{f}}{2}\rho_\mathrm{v}(u_\mathrm{v}-u_{\mathrm{l},i\delta})^2, \tag{18b}$$

where the two-phase flow friction coefficient, c_f, is given by [16]:

$$c_\mathrm{f}/2 = (c_\mathrm{f}/2)^*(1+850F), \tag{19}$$

with

$$(c_\mathrm{f}/2)^* = \frac{0.085}{Re_\mathrm{v}^{0.25}}, \quad F = \frac{\gamma\mu_R}{\rho_R^{0.5}Re_\mathrm{v}^{0.9}} \quad \text{and}$$
$$\gamma = [(1.414Re_\mathrm{l}^{0.5})^{2.5} + (0.132Re_\mathrm{l}^{0.9})^{2.5}]^{0.4}.$$

The velocity along the axial direction in the condensate film, $u_{\mathrm{l,i}}$, can then be obtained by integrating Eq. (10) subject to the boundary conditions of Eqs. (11), thus providing

$$u_{\mathrm{l,i}} = \frac{1}{4\mu_\mathrm{l}}\left(\frac{\partial p_{\mathrm{l,i}}}{\partial z}-\rho_\mathrm{l}g\right)(r_\mathrm{i}^2-R_\mathrm{i}^2) - \left[\frac{1}{\mu_\mathrm{l}}\tau_{\delta,\mathrm{i}}(R_\mathrm{i}-\delta_{\mathrm{l,i}}) + \frac{1}{2\mu_\mathrm{l}}\left(\frac{\partial p_{\mathrm{l,i}}}{\partial z}-\rho_\mathrm{l}g\right)(R_\mathrm{i}-\delta_{\mathrm{l,i}})^2\right]\ln\frac{r_\mathrm{i}}{R_\mathrm{i}}. \tag{20}$$

Assuming that the latent heat caused by condensation is balanced by heat conduction through the liquid film, we have:

$$\mathrm{d}\dot{m}_{\mathrm{l,i}} = \frac{\lambda_\mathrm{l}}{h_\mathrm{lv}} + \frac{T_\mathrm{s}-T_\mathrm{w}}{\ln\frac{R_\mathrm{i}}{R_\mathrm{i}-\delta_{\mathrm{l,i}}}}\mathrm{d}z\cdot\mathrm{d}\theta_\mathrm{i}. \tag{21}$$

Note that the increment of the condensate mass rate, $\mathrm{d}\dot{m}_{\mathrm{l,i}}$, is balanced by the variation of the downward flow rate of the condensate in the z-direction, $\mathrm{d}\dot{m}_{\mathrm{l,ui}}$, and the flow rate of the condensate along the circumference toward the meniscus zone, $\mathrm{d}\dot{m}_{\mathrm{l,vi}}$, i.e.:

$$\mathrm{d}\dot{m}_{\mathrm{l,i}} = \mathrm{d}\dot{m}_{\mathrm{l,vi}} + \mathrm{d}\dot{m}_{\mathrm{l,ui}}, \tag{22}$$

where

$$\mathrm{d}\dot{m}_{\mathrm{l,vi}} = \frac{\partial}{r_\mathrm{i}\partial\theta_\mathrm{i}}\left(\rho_\mathrm{l}\int_{R_\mathrm{i}-\delta_{\mathrm{l,i}}}^{R_\mathrm{i}} v_{\mathrm{l,i}}\mathrm{d}r_\mathrm{i}\cdot\mathrm{d}z\right)r_\mathrm{i}\,\mathrm{d}\theta_\mathrm{i} \tag{23a}$$

and

$$\mathrm{d}\dot{m}_{\mathrm{l,ui}} = \frac{\partial}{\partial z}\left(\rho_\mathrm{l}\int_{R_\mathrm{i}-\delta_{\mathrm{l,i}}}^{R_\mathrm{i}} u_{\mathrm{l,i}}\mathrm{d}r_\mathrm{i}\cdot r_\mathrm{i}\mathrm{d}\theta_\mathrm{i}\right)\mathrm{d}z. \tag{23b}$$

Substituting Eq. (14) into Eq. (23a) for $v_{\mathrm{l,i}}$ and Eq. (20) into Eq. (23b) for $u_{\mathrm{l,i}}$, we obtain:

$$\mathrm{d}\dot{m}_{\mathrm{l,vi}} = \frac{\partial}{r_\mathrm{i}\partial\theta_\mathrm{i}}\left\{\rho_\mathrm{l}\left[\frac{1}{\mu_\mathrm{l}}\frac{\partial p_{\mathrm{l,i}}}{\partial\theta_\mathrm{i}}\left(\frac{1}{2}r_\mathrm{i}^2\ln\frac{r_\mathrm{i}}{R_\mathrm{i}-\delta_{\mathrm{l,i}}} - R_\mathrm{i}\ln\frac{R_\mathrm{i}}{R_\mathrm{i}-\delta_{\mathrm{l,i}}}\cdot r_\mathrm{i} + R_\mathrm{i}r_\mathrm{i} - \frac{3}{4}r_\mathrm{i}^2\right)\right]\Bigg|_{R_\mathrm{i}-\delta_{\mathrm{l,i}}}^{R_\mathrm{i}}\right\}\mathrm{d}z\cdot r_\mathrm{i}\mathrm{d}\theta_\mathrm{i} \tag{24a}$$

and

$$\mathrm{d}\dot{m}_{\mathrm{l,ui}} = \frac{\partial}{\partial z}\left\{\rho_\mathrm{l}\left[\frac{1}{16\mu_\mathrm{l}}C_0r_\mathrm{i}^4 + \frac{C_1}{\mu_\mathrm{l}}\left(\frac{1}{2}r_\mathrm{i}^2\ln r_\mathrm{i} - \frac{1}{4}r_\mathrm{i}^2\right) + \frac{1}{2}C_2r_\mathrm{i}^2\right]\Bigg|_{R_\mathrm{i}-\delta_{\mathrm{l,i}}}^{R_\mathrm{i}}\right\}\mathrm{d}\theta_\mathrm{i}\,\mathrm{d}z, \tag{24b}$$

where

$$C_0 = \frac{\partial p_{\mathrm{l,i}}}{\partial z} - \rho_\mathrm{l}g;$$
$$C_1 = -\tau_{\delta,\mathrm{i}}(R_\mathrm{i}-\delta_{\mathrm{l,i}}) - \frac{1}{2}C_0(R_\mathrm{i}-\delta_{\mathrm{l,i}})^2;$$
$$C_2 = -\frac{1}{4\mu_\mathrm{l}}C_0R_\mathrm{i}^2 - \frac{C_1}{\mu_\mathrm{l}}\ln R_\mathrm{i}.$$

Substituting, respectively, Eq. (13) into Eq. (24a), Eq. (17) into Eq. (24b), as well as Eqs. (21) and (24) into Eq. (22), we obtain a partial differential equation for the local film thickness distribution, $\delta_{\mathrm{l,i}}(\theta_\mathrm{i})$, in terms of the axial distance, z, and the azimuth coordinate, θ_I as follows:

$$\frac{\lambda_\mathrm{l}}{h_\mathrm{lv}} + \frac{T_\mathrm{s}-T_\mathrm{w}}{\ln\frac{R_\mathrm{i}}{R_\mathrm{i}-\delta_{\mathrm{l,i}}}}\mathrm{d}z\cdot\mathrm{d}\theta_\mathrm{i} = \frac{\partial}{r_\mathrm{i}\partial\theta_\mathrm{i}}\left\{\rho_\mathrm{l}\left[\frac{-1}{\mu_\mathrm{l}}\left(\frac{\sigma_\mathrm{lv}}{(R_\mathrm{i}-\delta_{\mathrm{l,i}})^2}\frac{\partial\delta_{\mathrm{l,i}}}{\partial\theta_\mathrm{i}}\right)\times\left(\frac{1}{2}r_\mathrm{i}^2\ln\frac{r_\mathrm{i}}{R_\mathrm{i}-\delta_{\mathrm{l,i}}} - R_\mathrm{i}\ln\frac{R_\mathrm{i}}{R_\mathrm{i}-\delta_{\mathrm{l,i}}}\cdot r_\mathrm{i} + R_\mathrm{i}r_\mathrm{i} - \frac{3}{4}r_\mathrm{i}^2\right)\right]\Bigg|_{R_\mathrm{i}-\delta_{\mathrm{l,i}}}^{R_\mathrm{i}}\right\}\mathrm{d}z\cdot r_\mathrm{i}\mathrm{d}\theta + \frac{\partial}{\partial z}\left\{\rho_\mathrm{l}\left[\frac{1}{16\mu_\mathrm{l}}C_0r_\mathrm{i}^4 + \frac{C_1}{\mu_\mathrm{l}}\left(\frac{1}{2}r_\mathrm{i}^2\ln r_\mathrm{i} - \frac{1}{4}r_\mathrm{i}^2\right) + \frac{1}{2}C_2r_\mathrm{i}^2\right]\Bigg|_{R_\mathrm{i}-\delta_{\mathrm{l,i}}}^{R_\mathrm{i}}\right\}\mathrm{d}\theta_\mathrm{i}, \tag{25a}$$

where

$$C_0 = (\rho_\mathrm{v}-\rho_\mathrm{l})g - \frac{\tau_{\delta,\mathrm{i}}P_\mathrm{w}}{A_\mathrm{v}} + \frac{\sigma_\mathrm{lv}}{(R_\mathrm{i}-\delta_{\mathrm{l,i}})^2} + \frac{\mathrm{d}(R_\mathrm{i}-\delta_{\mathrm{l,i}})}{\mathrm{d}z};$$
$$C_1 = -\tau_{\delta,\mathrm{i}}(R_\mathrm{i}-\delta_{\mathrm{l,i}}) - \frac{1}{2}C_0(R_\mathrm{i}-\delta_{\mathrm{l,i}})^2 \quad \text{and}$$
$$C_2 = -\frac{1}{4\mu_\mathrm{l}}C_0R_\mathrm{i}^2 - \frac{C_1}{\mu_\mathrm{l}}\ln R_\mathrm{i}.$$

Eq. (25a) can be solved subject to the following boundary conditions:

$$\theta_\mathrm{i} = 0 : \frac{\partial\delta_{\mathrm{l,i}}}{\partial\theta_\mathrm{i}} = 0, \tag{25b}$$

$$\theta_i = \Theta_{i,m} : -\frac{\partial \delta_{l,i}}{\partial \theta_i} = \frac{\partial r_m}{\partial \theta_m}. \tag{25c}$$

Note that Eq. (25b) reflects the fact that the liquid film is symmetric with respective to point A (see Fig. 1), while Eq. (25c) is due to the assumption that the thin liquid film at point B is tangential to the arc of the liquid–vapor interface within the meniscus zone.

2.2. Condensation in the meniscus zone

The liquid motion within the meniscus zone is treated as a one-dimension flow [2,10]. The conservation equation of momentum can be expressed as

$$\frac{\rho_l}{A_{l,m}} \frac{d}{dz}(\bar{u}_{l,m}^2 A_{l,m}) = -\frac{dp_{l,m}}{dz} + \rho_l g + \frac{\tau_{\delta,m} P_{l,m}}{A_{l,m}} - \frac{\tau_{w,m} P_{w,m}}{A_{l,m}}, \tag{26}$$

where $\bar{u}_{l,m}$ is the mean condensate velocity in the meniscus zone, $P_{l,m}$ and $P_{w,m}$ are the wetted perimeters along the tube wall and liquid–vapor interface within the meniscus zone, respectively. Note that $P_{l,m}$ and $P_{w,m}$ can be expressed as functions of r_m and $\delta_{l,i}$ at point B.

The variation of the condensate mass flow rate in the meniscus zone is balanced by the condensing mass flow rate, $d\dot{m}_{l,cm}$, and the condensate liquid flowing toward the meniscus zone induced by the capillary force, $d\dot{m}_{l,vm}$, i.e.:

$$\rho_l d(\bar{u}_{l,m} A_{l,m}) = d\dot{m}_{l,vm} + d\dot{m}_{l,cm}, \tag{27}$$

where

$$d\dot{m}_{l,vm} = \int_{R_i-\delta_{l,i}}^{R_i} \rho_l v_{l,i}\, dr_i \Big|_{\theta_i=\Theta_{i,m}} \tag{28}$$

and $d\dot{m}_{l,cm}$ can be determined from the energy balance as follows:

$$h_{lv} d\dot{m}_{l,cm} = h_{l,m} P_{w,m} (T_s - T_w) dz, \tag{29}$$

with the local condensation heat transfer coefficient, $h_{l,m}$, given by [18]:

$$h_{l,m} = \frac{\left(\frac{dp_v/dz}{dp_{l,m}/dz}\right)^{0.5} \left(\frac{\lambda_l}{D_h}\right) \left(\frac{8\rho_l u_{l,m} D_h}{\mu_l}\right)^{0.5}}{5 + 5[\ln(5Pr_l + 1)] Pr_l^{-1}}. \tag{30}$$

To formulate the film condensation heat transfer inside the flow passage formed by welding a thin metal wire on the inner wall of a round micro tube, we have presented major equations in the preceding sections. To close the problem, one more parameter, i.e., the meniscus interface radius, r_m, is needed to determine the cross-section area of the meniscus zone, A_{lm}, and the other geometric parameters, which are discussed in the following section.

2.3. Determination of the liquid–vapor interface within the meniscus zone

The minimum energy principle over the two-phase flow system considered is employed to determine the liquid–vapor interface radius, r_m, within the meniscus zone. In the case of flow condensation in a mini channel, in addition to gravity and shear stress, the capillary force due to the surface tension also plays an important role at the liquid–vapor interface. The distribution of liquid condensate inside the flow passage depends on the resultant of these three forces exerted on the two-phase flow system. Of these, gravity and shear stress lead to the kinetic energy, E_k, while the capillary force causes the surface energy, E_s, of the system. For a steady phase equilibrium system, the most possible condensate liquid distribution along the periphery of the channel should satisfy the minimum energy principle. Thus, the meniscus interface radius, r_m, can be obtained as follows.

For a unit length of the tube, the kinetic energy, E_k, consists of three components, i.e.:

$$E_k = E_{k,i} + E_{k,m} + E_{k,v}, \tag{31}$$

where

$$E_{k,i} = \int_0^{\Theta_{i,m}} \int_{R_i-\delta_{l,i}}^{R_i} \frac{1}{2} \rho_l u_{l,i}^2 r_i\, dr_i\, d\theta_i + \int_{R_i-\delta_{l,i}}^{R_i} \int_0^{\Theta_{i,m}} \frac{1}{2} \rho_l v_{l,i}^2 r_i\, dr_i\, d\theta, \tag{32}$$

is the kinetic energy in the thin liquid film zone,

$$E_{k,m} = \frac{1}{2} \rho_l A_{l,m} \bar{u}_{l,m}^2, \tag{33}$$

is the kinetic energy in the meniscus liquid zone, and

$$E_{k,v} = \frac{1}{2} \rho_v A_v u_v^2, \tag{34}$$

is the kinetic energy in the vapor core flow zone.

Assuming that the liquid–vapor interface is smooth, we can express the surface energy of the two-phase flow system as

$$E_s = \sigma_{lv}[(R_i - \delta_{l,i})\Theta_{i,m} + r_m \Theta_m] + \sigma_{lw}(\pi R_i + R_o \Theta_{o,m}) + \sigma_{vw}(\pi R_o - R_o \Theta_{o,m}). \tag{35a}$$

Applying the Young's equation [17] to Eq. (35a), we have

$$E_s = \sigma_{lv}[(R_i - \delta_{l,i})\Theta_{i,m} + r_m \Theta_m] - \cos\alpha \sigma_{lv} R_o \Theta_{o,m} + \sigma_{lw}(\pi R_i) + \sigma_{vw}(\pi R_o). \tag{35b}$$

It should be recognized that the last two terms in Eq. (35b) are independent of the area of the meniscus zone or r_m and thus, they go to nil when they are differentiated with respect to r_m.

The total energy over the system can be then obtained from

$$E_T = E_{k,i} + E_{k,m} + E_{k,v} + E_s. \tag{36}$$

Based on the minimum energy principle, the interface radius of the meniscus zone, r_m, should satisfy the following condition, corresponding to the most possible distribution of the condensate liquid

$$\frac{dE_T}{dr_m} = 0, \tag{37}$$

r_m can now be obtained from Eq. (37).

2.4. Determination of vapor quality and heat transfer rates

The vapor quality, x, at the axial position, z, is defined as

$$x = \frac{\dot{m}_v}{\dot{m}_{v0}}, \tag{38}$$

where $\dot{m}_{v0} = \frac{1}{2}\rho_v A_T u_{v0}$ and $\dot{m}_v = \dot{m}_{v0} - \dot{m}_l = \dot{m}_{v0} - (\dot{m}_{l,i} + \dot{m}_{l,cm})$, with $\dot{m}_{l,i}$ and $\dot{m}_{l,cm}$ determined by integrating Eqs. (21) and (29) with z. The local heat transfer coefficient in the thin condensate liquid film zone is defined as

$$h_{l,i} = \frac{\lambda_l}{\ln \dfrac{R_i}{R_i - \delta_{l,i}}}. \tag{39}$$

The average Nusselt number, Nu, over the entire cross-section at the axial position, z, is determined from

$$Nu = \frac{\left[\int_0^{\Theta_{i,m}} h_{l,i}(R_i - \delta_{l,i})\,d\theta_i + h_{l,m}\Theta_m r_m\right] \Big/ P_w D_h}{\lambda_l}. \tag{40}$$

3. Numerical scheme

We now outline the numerical calculation procedures as follows:

(1) Discretize the governing equations, Eqs. (7), (8), (10), (21) and (26), as well as the associated boundary conditions using the backward finite difference scheme in the thin liquid film zone and the meniscus zone;
(2) At every axial step, Δz, giving initial values for both the interface radius of the condensate liquid in the meniscus corner zone, r_m, and also, the azimuthal angle characterizing the width of the thin film zone, $\Theta_{i,m}$, solve Eq. (25a) subject to the boundary conditions to determine the circumferential profile of the condensate liquid in the thin film zone by applying Eqs. (13), (17) and (18) to obtain τ_δ and the pressure gradients, $\frac{\partial p_{l,i}}{\partial \theta_i}$ and $\frac{\partial p_{l,i}}{\partial z}$;
(3) Calculate the new value of $\Theta_{i,m}$ based on the value of $\delta_{l,i}$ at $\theta_i = \Theta_{i,m}$ obtained in the preceding step, and then determine the other geometric parameters from Eqs. (1)–(6);
(4) Check whether the first-guessed $\Theta_{i,m}$ equals to the new value obtained in step (3). If not, modify the initial value of $\Theta_{i,m}$ and repeat the steps (2) and (3);
(5) Solve Eqs. (31)–(36) to obtain the system energy;
(6) Check again whether the first-guessed interface radius of meniscus zone, r_m, satisfies the minimum energy principle by Eq. (37). If not, modify the initial value of r_m and repeat steps (2)–(5).
(7) Calculate the vapor quality and the Nusselt number at the current axial step, Δz, by Eqs. (38) and (40), and then begin the solution of the next axial step. The numerical calculation procedure is terminated as the vapor quality, x, becomes less than 0.05.

4. Results and discussion

The typical results are presented for condensation heat transfer in a vertical mini round tube with a thin metal wire welded on its inner surface. Unless otherwise noted, all the results presented in the following are for condensation of the water vapor in a tube with an inside diameter of 0.5 mm and a wire with the diameter of 0.1 mm under the conditions of the same inlet vapor Reynolds number, $Re_{v0}(=\rho_v u_{v0} D_h/\mu_v) = 1800$, and the same subcooling, $T_s - T_w = 5$ K. The effects of the metal wire size and its surface wettabilities are also examined.

The variations in the total energy over the two-phase flow system within the cross-section area of the meniscus zone for different vapor qualities are presented in Fig. 2, where E_{T0} represents the total energy of the pure vapor flow at the inlet. Fig. 2a–d, each corresponding to a fixed vapor quality, show that with an increase in the cross-sectional area of the meniscus zone, the total energy of the system decreases, reaches a minimum value, and then increases afterwards. This behavior clearly indicates that there always exists a definite cross-sectional area of the meniscus zone, A_{lm}, at which the two-phase flow system reaches its minimum energy. And any deviation from this equilibrium point causes an increase in the total energy. This equilibrium point then corresponds to the most possible distribution of the liquid over the two-phase system during the vapor condensation. Accordingly, the liquid–vapor interface radius, r_m, of the meniscus zone can be determined based on the equilibrium cross-sectional area of the meniscus zone.

The variations in the azimuthal angles, $\Theta_{i,m}$ and $\Theta_{o,m}$, characterizing the width of the thin film zone and that of the meniscus zone, respectively, along the axial distance are illustrated in Fig. 3. It can be seen that both $\Theta_{i,m}$ and $\Theta_{o,m}$ decrease with the axial distance, implying that the meniscus zone becomes progressively larger, and that

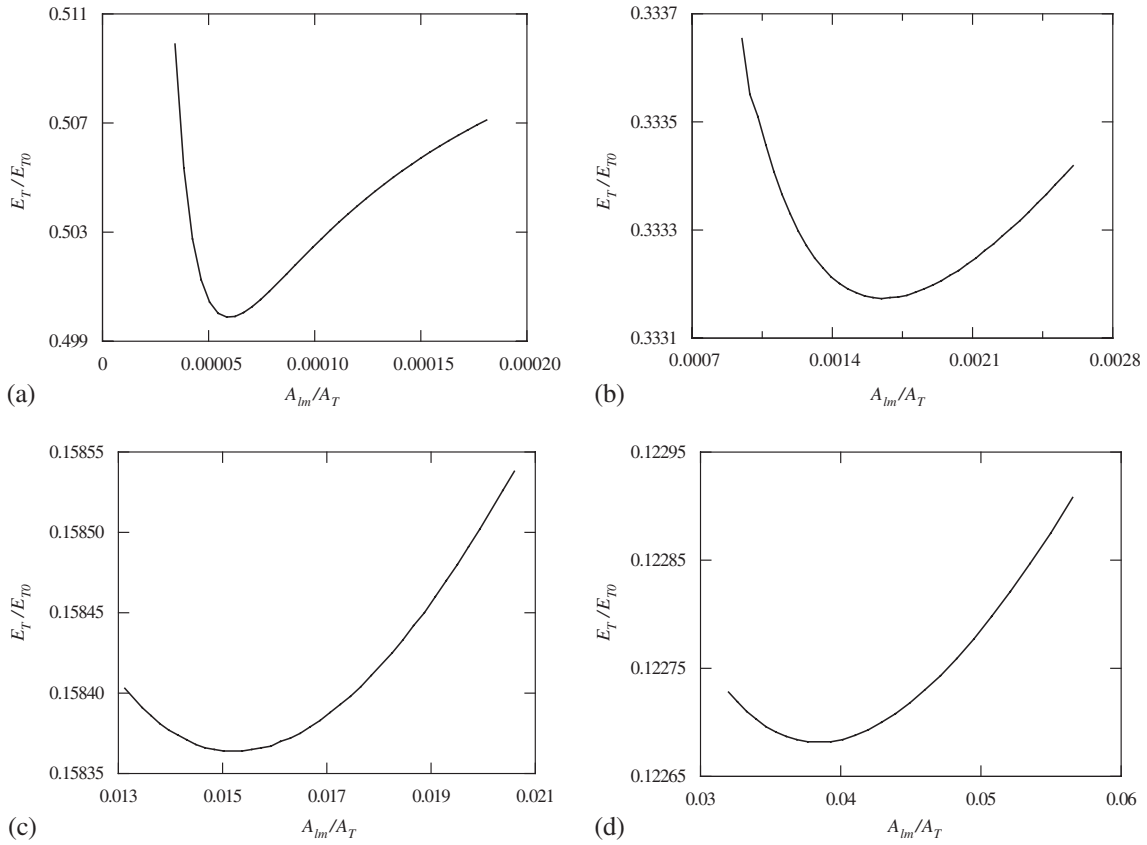

Fig. 2. Variations in the total energy with the meniscus zone cross-section area for different vapor qualities ($D_i = 0.5$ mm; $D_o = 0.1$ mm; $\alpha = 45°$). (a) $x = 0.88$; (b) $x = 0.68$; (c) $x = 0.37$; (d) $x = 0.27$.

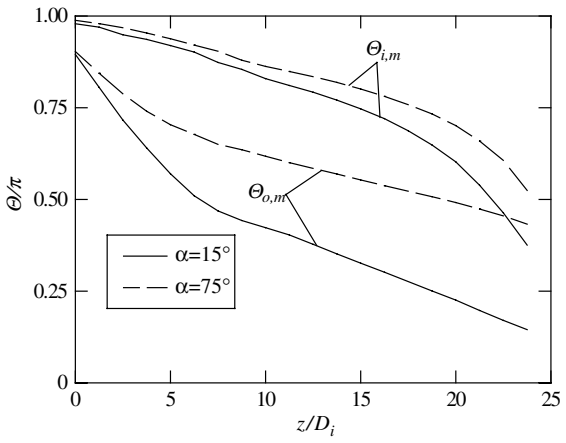

Fig. 3. Variations in the azimuthal angles $\Theta_{i,m}$ and Θ_m, along the axial distance for different contact angles between condensate and metal wire ($D_i = 0.5$ mm; $D_o = 0.1$ mm).

the thin liquid film zone becomes narrower towards the exit of the flow passage. Fig. 3 also indicates that when the contact angle between the fluid and the wire is increased, the decrease of $\Theta_{i,m}$ and $\Theta_{o,m}$ becomes slower. This behavior reflects the fact that as the wettability of the wire is reduced, the meniscus effect draining the liquid towards the meniscus zone becomes less pronounced.

Fig. 4 presents the condensate thickness distribution within the thin liquid film zone along the tube periphery (i.e.: $0 < \theta_i < \Theta_{i,m}$) for selected vapor qualities. The liquid film profiles show that the condensate becomes thicker with an increase in the azimuth, θ_i, for all the selected vapor qualities. As the vapor condenses progressively along the downstream, the film thickness in the thin film zone also increases, and is accompanied by a decrease in the vapor quality. It is also seen from Fig. 4 that as it approaches to the meniscus zone ($\theta_i \to \Theta_{i,m}$), the variation in the film thickness becomes much sharper, indicating that the meniscus draining effect becomes more pounced near the meniscus zone.

Fig. 5 presents the variations in the cross-sectional area of the meniscus zone along the axial distance for different contact angles between the metal wire and the condensate liquid. It can be seen that the cross-sectional area of the meniscus zone increases for all the contact

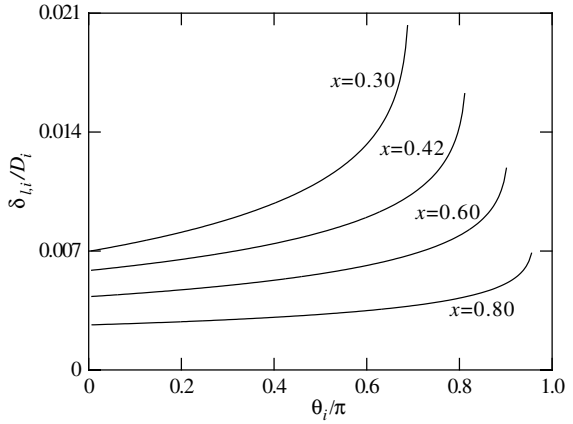

Fig. 4. Profiles of the condensate film thickness in the thin liquid film zone for various vapor qualities ($D_i = 0.5$ mm; $D_o = 0.1$ mm; $\alpha = 45°$).

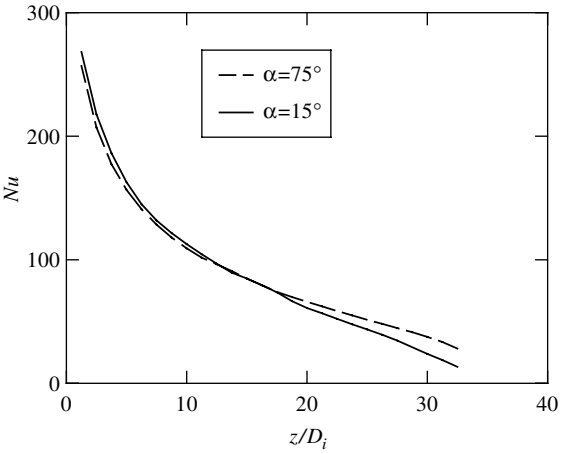

Fig. 6. Effects of the contact angle on the Nusselt number ($D_i = 0.5$ mm; $D_o = 0.1$ mm).

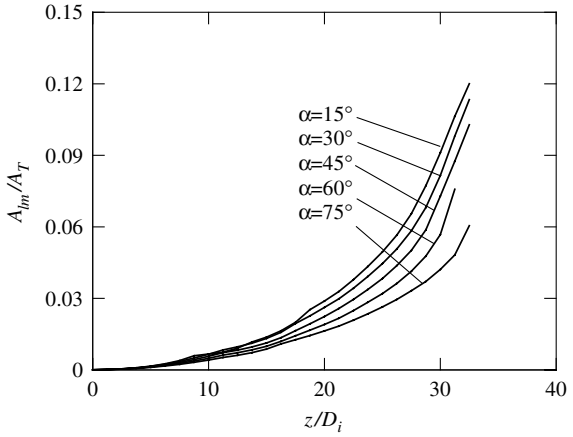

Fig. 5. Effects of the contact angle on the variations in the meniscus zone cross-section area along the axial distance ($D_i = 0.5$ mm; $D_o = 0.1$ mm).

angles with the axial distance, implying that more condensate liquid is drawn into the meniscus zone towards the exit of the flow passage. It is also evident from Fig. 5 that the meniscus zone becomes smaller with an increase in the contact angle due to the fact that the draining effect of the meniscus becomes weaker as the wettability of the wire is weakened.

The variations in the average Nusselt numbers, defined in Eq. (40), along the axial distance for different contact angles between the wire and the condensate are shown in Fig. 6. The Nusselt number is seen to decrease with the axial distance because the liquid film becomes progressively thicker towards the exit of the flow passage to increase the thermal resistance. It is also interesting to note that a wire with a higher wettability (corresponding to a smaller contact angle) leads to a higher heat transfer rate in the entrance region of the flow passage. However, further downstream towards the exit of the flow passage, the heat transfer rate for a wire with a higher wettability becomes smaller than that for a wire with a lower wettability. This behavior can be explained as follows: As shown in Eq. (40), the Nusselt numbers presented in Fig. 6 were obtained by averaging the heat transfer rates in the thin liquid film zone and the meniscus zone, the overall heat transfer rates in the entrance region of the flow passage are dominated by the thin liquid film zone, while in the exit region of the flow passage the meniscus zone will play a more important role for heat transfer. The wire with a higher wettability leads to a thinner liquid film in the entrance region and thus to higher heat transfer rates. However, in the downstream towards the exit, the wire with a higher wettability will lead to an increase of the area of the meniscus zone (see Fig. 5). The condensate flow in the meniscus zone is found to be quite similar to the accumulated condensate flow at the lower part of the tube for the stratified flow in a horizontal tube [2], where the heat transfer coefficients are relatively low. Thus, the wire with a higher wettability results in lower heat transfer rates in the downstream of the flow passage.

The effects of the metal wire diameter on the cross-sectional area of the meniscus zone and the condensate thickness in the thin liquid film zone are compared for the same inlet vapor Reynolds number, Re_{v0} in Figs. 7 and 8. It is seen from Fig. 7 that the cross-section area of the meniscus zone increases when the diameter of the metal wire increases, meaning that more condensate liquids can be drained into the meniscus zone for a wire with a large diameter. Therefore, we can conclude that the draining effect formed in the meniscus zone becomes more significant for the condensate liquid distribution as

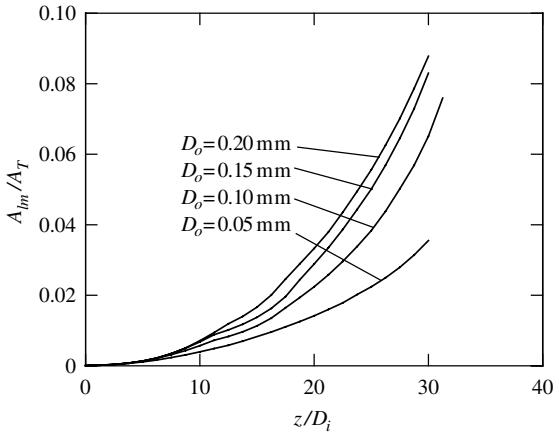

Fig. 7. Effects of the metal wire diameter on the cross-sectional area of the meniscus zone ($D_i = 0.5$ mm; $\alpha = 45°$).

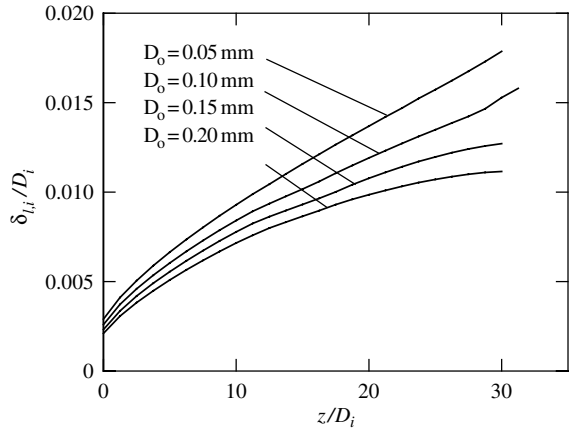

Fig. 8. Effects of the metal wire diameter on the average thickness of the condensate liquid in the thin film zone ($D_i = 0.5$ mm; $\alpha = 45°$).

the metal wire size is increased. Because of the increased draining effect for larger wires, it is seen from Fig. 8 that the condensate film thickness in the thin film zone becomes thinner as the wire size is increased.

Fig. 9 presents the effect of the wire size on the average Nusselt number, Nu, along the axial distance at the same inlet vapor Reynolds number, Re_{v0}. It is clear from Fig. 9 that the tube without welding a metal wire welded on its inner surface (i.e., the bare tube) exhibits the smallest Nusselt numbers at the maximum vapor quality region, whereas the tube with the largest wire has the highest Nusselt numbers. The heat transfer enhancement is attributed to the fact that the liquid film becomes thinner when a larger wire is adapted, which is shown in Fig. 8. On the other hand, it is also observed that the heat transfer enhancement induced by the larger wire becomes progressively insignificant toward the exit of

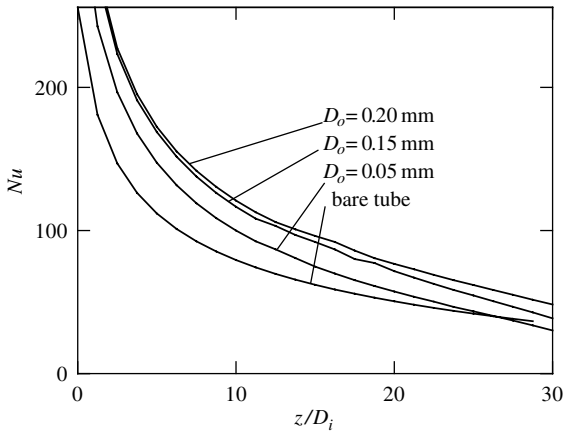

Fig. 9. Effects of the metal wire diameter on the Nusselt number ($D_i = 0.5$ mm; $\alpha = 45°$).

the flow passage. This is due to the fact that when the vapor quality along the axial distance is reduced, the thin liquid film zone becomes smaller, whereas the meniscus zone becomes larger, which weakens the heat transfer enhancement because of the low surface heat transfer coefficients on the meniscus zone.

5. Concluding remarks

In this work we have introduced a new non-circular microchannel, formed by a circular micro tube with a thin metal wire welded on its inner surface. The formation of this non-circular microchannel is simple and inexpensive. We have investigated theoretically the film condensation heat transfer in this type of non-circular microchannels, taking into consideration the meniscus draining effect, formed by the wire in contact with the tube inner wall. Both the radial and axial distributions of condensate liquid along the tube wall and over the meniscus zone are determined by solving the simplified conservation equations of mass and momentum for the liquid and vapor phases, combined with the minimum energy principle for a two-phase flow system in order to determine the meniscus zone configuration. We have examined the influences of the contact angle between the condensate liquid and channel wall, together with the influences of the wire size on the condensate distribution and the heat transfer characteristics. It is found that an increase in the wire diameter welded on the channel inner surface has a significant effect on the fluid flow and heat transfer within the channel. It is also demonstrated that the wettability between the wire and the condensate has a minor influence on the overall heat transfer rates. Compared to a round tube with the same inside diameter, significant enhancement in condensation heat transfer is found for the present configured channel.

Acknowledgements

The work described in this paper was fully supported by a grant from the Research Grants Council of the Hong Kong Special Administrative Region, China (project no. HKUST6193/01E).

References

[1] L.A. Guntly, N.F. Costello, US Patent no. 4998580, 1991.
[2] T.S. Zhao, Q. Liao, Theoretical analysis of film condensation heat transfer inside vertical mini triangular channels, Int. J heat Mass Transfer 45 (2002) 2829–2842.
[3] D. Khrustalev, A. Faghri, Thermal analysis of a micro-heat pipe, ASME J. Heat Transfer 116 (1994) 189–198.
[4] Y.W. Zhang, A. Faghri, Numerical simulation of condensation on a capillary grooved structure, Numer. Heat Transfer A—Appl. 39 (2001) 227–243.
[5] V. Sartre, M.C. Zaghdoudi, M. Lallemand, Effect of interfacial phenomena on evaporative heat transfer in micro heat pipes, Int. J. Thermal Sci. 39 (2000) 498–504.
[6] C.B. Sobhan, X.Y. Huang, L.C. Yu, Investigations on transient and steady-state performance of a micro heat pipe, J. Thermophys. Heat Transfer 14 (2000) 161–169.
[7] L.W. Swanson, G.P. Peterson, The interfacial thermodynamics of micro heat pipes, ASME J. Heat Transfer 117 (1995) 195–201.
[8] J.M. Ha, G.P. Peterson, The heat transport capacity of micro heat pipes, ASME J. Heat Transfer 120 (1998) 1064–1071.
[9] G.P. Peterson, H.B. Ma, Temperature response of heat transport in a micro heat pipe, ASME J. Heat Transfer 121 (1999) 438–445.
[10] G.P. Peterson, H.B. Ma, Theoretical analysis of the maximum heat transport in triangular grooves: a study of idealized micro pipes, ASME J. Heat Transfer 118 (1996) 731–739.
[11] C.Y. Yang, A critical review of condensation heat transfer predicting models-effects of surface-tension force, J. Enhanced Heat Transfer 6 (1999) 217–236.
[12] C.Y. Yang, R.L. Webb, A predictive model for condensation in small hydraulic diameter tubes having axial microfins, ASME J. Heat Transfer 119 (1997) 776–782.
[13] R.L. Webb, M. Zhang, Heat transfer and friction in small diameter channels, Microscale Thermophys. Eng. 2 (1998) 189–202.
[14] W. Wang, T.D. Radcliff, R.N. Christensen, A condensation heat transfer correlation for millimeter-scale tubing with flow regime transition, Exp. Thermal Fluid Sci. 26 (2002) 473–485.
[15] A. Tabatabai, A. Faghri, A new two-phase flow map and transition boundary accounting for surface tension effects in horizontal miniature and micro tubes, ASME J. Heat Transfer 123 (2001) 958–968.
[16] W.H. Henstock, T.J. Hodgson, The interfacial drag and height of the wall layer in annular flows, AIChE J. 22 (1976) 990–1000.
[17] A.W. Adamson, A.P. Gast, Physical Chemistry of Surface, John Wiley & Sons, New York, 1997.
[18] I.Y. Chen, G. Kocamustafaogullari, Condensation heat transfer studies for stratified, cocurrent two-phase flow in horizontal tubes, Int. J. Heat Mass transfer 30 (1987) 1133–1148.